

Graphitic-C₃N₄ coated floating glass beads for photocatalytic destruction of synthetic and natural organic compounds in water under UV light

Jianing Hui ^{a*}, Carlos J. Pestana ^b, Marine Caux ^a, H. Q. Nimal Gunaratne ^c, Christine Edwards ^b, Peter K. J. Robertson ^c, Linda A. Lawton ^b and John T. S. Irvine ^{a*}

^a School of Chemistry, University of St Andrews, North Haugh, St Andrews, Scotland, KY16 9ST, UK.

^b School of Pharmacy and Life Sciences, Robert Gordon University, Garthdee Road, Aberdeen, Scotland, AB10 7GJ, UK.

^c School of Chemistry and Chemical Engineering, the Queen's University of Belfast, Steanmillis Road, Belfast, Northern Ireland, BT9 5AG, UK.

Keywords: g-C₃N₄, Floating photocatalysts, Microcystin-LR, Cylindrospermopsin, Dye degradation

Abstract:

Many drinking water reservoirs can contain organic pollutants such as artificial synthesized dye and drugs. On the other hand, some naturally occurring microorganisms such as cyanobacteria, are capable of producing toxic secondary metabolites (cyanotoxins) causing detrimental health effects in humans and animals are also present in water reservoirs. Photocatalytic destruction of organic pollutants in-reservoir requires not only good photo-catalytically activity but also efficacy of distribution and recycling. We report here, a facile calcination method of coating graphitic carbon nitride (g-C₃N₄) onto porous glass beads. Influences of precursor and heating temperature on photocatalytic activity were evaluated by photocatalytic degradation of methyl orange. The yellow floating beads show comparable activity to P25 (TiO₂) coated beads in the removal of two of the most frequently occurring cyanobacterial toxins, microcystin-LR and cylindrospermopsin, in artificial freshwater under UV light irradiation. Microcystin-LR was destroyed within 60 min and cylindrospermopsin was removed after 100 min UV irradiation. The coated g-C₃N₄ layer is very robust and shows negligible degradation on photocatalytic

performance when recycled. The recycling of the photocatalyst is very simple because of the large size of the catalyst-coated beads. A large batch was successfully produced in a lab tube furnace. For further application, the ability of $g\text{-C}_3\text{N}_4$ absorbing visible light could pave the way to utilise sunlight for the destruction of toxins in the water.

1. Introduction

Drinking water contamination caused by organic pollutants has been a worldwide concern. Synthetic pollutants that created as a result of human activity are easy to control by cutting off the pollution sources, while some organic compounds generated in nature are more complicated to deal with. Cyanotoxins due to algae blooms is one of the major threat to the safety of drinking water, especially in some developing countries.¹ A large number of studies have been carried out on cyanobacterial toxin monitoring and management. Microcystin-LR (MC-LR) and cylindrospermopsin (CYL) are two of the most commonly occurring toxins found in reservoir water.² MC-LR, a member of a group containing over 240 congeners, is a cyclic heptapeptide with two variable amino acid residue positions (see Fig. S1a). MC-LR has been reported in many lakes/reservoirs that provide drinking water, negatively affecting water quality. CYL is a polycyclic uracil derivative which contains both guanidino and sulphate moieties (see Fig. S1b).³ Both toxins are known to be relatively stable compounds, which makes them difficult to remove by conventional treatment methods when dissolved in the raw water.

Photocatalytic destruction is a promising technology to remove cyanotoxins within the reservoir using solar energy directly.⁴ On the surface of a semiconductor photocatalyst, hydroxide ions are oxidised to hydroxyl radicals (OH^\bullet) at the valence band (VB). The photogenerated OH^\bullet radicals can oxidize a broad range of organic pollutants. Oxygen is reduced to superoxide radical anions ($\text{O}_2^{\bullet-}$) at the conduction band (CB). The $\text{O}_2^{\bullet-}$ anions may be protonated ultimately forming hydrogen peroxides (H_2O_2), both of which are also oxidizing agents.^{5, 6}

Graphitic carbon nitride ($g\text{-C}_3\text{N}_4$) is a metal-free semiconductor, possessing carbon and nitrogen atoms arranged based on a tri-s-triazine unit.^{7, 8} The ideal $g\text{-C}_3\text{N}_4$ is constructed from highly conjugated two-dimensional sheets with a graphitic structure in three-dimension. Because of the good thermal-, chemical-, and photostability of this material, as well as favourable band

positions [CB = -1.4 V, VB = 1.3 V vs. Ag/AgCl at pH 6.6], g-C₃N₄ is suitable for visible-light-driven water splitting and dye degradation.⁹⁻¹¹ There have been some investigations on the photocatalytic destruction of cyanobacterial toxins over the past few years.¹²⁻¹⁶ Only a few studies were about g-C₃N₄. Xu et al.¹⁶ reported g-C₃N₄/BiVO₄, a Z-scheme heterojunction, removed MC-LR efficiently under visible light using photo-generated hydroxyl radicals and superoxide radicals. However, the effect of a single g-C₃N₄ photocatalyst (i.e. without invoking composite systems incorporating toxic metals) in cyanobacterial toxins destruction has not been studied yet.

One of the major drawbacks to the wide application of photocatalyst in real water such as reservoirs and rivers is the size of the photocatalyst. Most of the reported high activity photocatalysts are in the size of micrometres or even nanometres. The direct use of this kind of fine powders in water has potential danger to the environment.^{17, 18} Moreover, most of these photocatalysts have a higher density than water, which means they will accumulate at the bottom of the reservoir in the absence of agitation. As light penetration is limited to the upper part of the water column obtaining light irradiation for these photocatalytic nanoparticles is problematic. One of the most promising strategies is to immobilize the active photocatalysts onto a floating substrate.¹⁹ Different types of substrates such as expanded perlite^{14, 15, 20}, fly ash beads²¹ and expanded polymer spheres²² have been used as photocatalysts substrates, however, these substrates have inherent disadvantages. For example, expanded perlite is very fragile because of its thin-walled structure. Coal fly ash is usually in micro-metre size, which is difficult to recover. The polymer substrates are also susceptible to degradation under UV light irradiation. Moreover, less stable substrates will further result in catalyst shedding during usage. Jingke Song et al.^{14, 15} reported effective inactivation of *Microcystis aeruginosa* (toxic cyanobacterium) using C₃N₄ and C₃N₄/TiO₂ immobilized on expanded perlite, however, the photocatalysts showed an obvious shedding after a non-stirring test.

In this work, we used expanded glass beads with a porous inner core but relative dense shell structure for g-C₃N₄ loading. These cheap glass beads are obtained during waste glass recycling and used as a lightweight building material. They present with good robustness and relatively regular surface for photocatalysts coating. A facile calcination method using a polymer precursor was used to obtain a g-C₃N₄ coating layer. Optimization on coating process was

carried out and the photocatalytic activity of obtained yellow floating photocatalysts was evaluated in dye degradation. To compare with the commercial TiO₂ (P25), P25 coated glass beads were prepared as a reference in the cyanobacterial toxin removal test.

2. Experimental

2.1 Materials and chemicals

Expanded glass beads (Diameter: 2~4 mm) were provided by Dennert Poraver GmbH (Germany). P25 (TiO₂, Rutile: Anatase/ 85: 15, 99.9%, 20 nm, from Aeroxide), thiourea (Sigma Aldrich, >99%), dicyandiamide (Sigma Aldrich, 99%), melamine (Sigma Aldrich, 99%) and ethylenediaminetetraacetic acid (EDTA, Sigma Aldrich, ACS reagent) were used as received. Isopropanol (2-propanol, ACS, 99.5%) was obtained from Alfa Aesar. Deionized (DI) water was used in all the experiment. MC-LR was obtained as per Edwards et al.²³, CYL was obtained from Enzo Life Science, USA. Artificial freshwater was prepared according to Akkanen and Kokkonen²⁴, in short CaCl₂ (58.8 mg L⁻¹), MgSO₄ (24.7 mg L⁻¹), NaHCO₃ (13.0 mg L⁻¹), and KCl (1.2 mg L⁻¹) were dissolved in ultrapure water (18.2 MΩ) and the pH adjusted to 7 with either HCl or NaOH (all chemicals were acquired from Fisher Scientific, UK).

2.2 Preparation of g-C₃N₄ coated glass beads

Glass beads (used as received) were washed in an ultrasonic bath (Ultrawave U300H, SLS, UK) to remove any potential surface contamination with acetone and DI water, respectively. Clean beads were dried in an oven at 80 °C for further coating. For g-C₃N₄ coating, wet beads (3 g) were mixed with the precursor (1.2 g) thoroughly to let the powder adhere to the surface of the bead. After that, the mixture was transferred into a custom-made aluminium crucible and covered with aluminium foil. The aluminium crucible was calcined in a muffle furnace at a temperature range from 450 to 600 °C. Post calcination the g-C₃N₄ coated beads were agitated gently in a stainless-steel sieve (pore size 1 mm) and washed with water thoroughly to remove unattached g-C₃N₄ particles. The loading amount is between 10 wt% and 15 wt% depending on different heating processes.

2.3 Preparation of P25 coated glass beads

The same pre-treatment as described for $g\text{-C}_3\text{N}_4$ coated glass beads was performed before coating with P25. The precursor turbid liquid was prepared by adding 1 g P25 nano-powder into 10 mL water. An ultrasonic bath was employed to break agglomeration and form a homogeneous suspension. Pre-treated glass beads were immersed into the precursor turbid liquid for 10 min with intermittent stirring. After this, the beads were removed from the precursor solution and dried in an oven at 80 °C. Coated beads were calcined at 550 °C to create a strong bonding between TiO_2 and the glass beads. Each cycle of coating deposited about 2 wt% TiO_2 catalyst. Repeated coatings were carried out to achieve a catalyst loading amount of more than 12 wt%. The beads used in the present work present with a TiO_2 loading of approximately 12 wt%. Photos in Fig. S2 show 100 g batch achieved in a lab tube furnace with a uniform coating of $g\text{-C}_3\text{N}_4$ and P25.

2.4 Characterization

The morphologies and elemental distribution analysis of coated glass beads were carried out on a scanning electron microscope (SEM, FEI Scios DualBeam) and its dispersive X-ray spectroscopy (EDX) module. The phase was confirmed by powder X-ray diffraction (XRD) on a PANalytical Empyrean X-ray diffractometer operated in reflection mode ($\text{Cu K}\alpha 1$). Glass beads were ground to a powder using a pestle and mortar before performing XRD analysis. UV-Vis absorbance spectra were collected on an ultraviolet-visible spectrophotometer (JASCO-V550). The BET (Brunauer-Emmett-Teller) surface area of samples was tested on a Micrometrics TriStarII 3020 instrument.

2.5 Catalyst evaluation by photocatalytic dye degradation

To optimize the $g\text{-C}_3\text{N}_4$ coating process on glass beads, a custom-made multi-channels photoreactor was employed to run photocatalytic dye degradation experiments. As shown in Fig. S3a, a maximum of eight glass vial can be held in this reactor by a glass vial holder. A Fe doped metal halide lamp (250 W) was fixed 15 cm above the vial holder. To allow the same amount of light irradiation for each sample, a DC gear motor was used to rotate vial holder gently at a speed of 10 rpm. Cooling fans were fixed beside glass vials to maintain the

temperature at 25 °C during the reaction. Each glass vial was covered by a thin quartz glass window to prevent water evaporation. For methyl orange (MO) degradation, each glass vial was filled with 25 mL 6.5 mg·mL⁻¹ (0.02 mM) MO aqueous solution. The quenchers (isopropanol, ethylenediaminetetraacetic acid) were added by a volume ratio 1:100 to the solution. Samples (500 µL) were withdrawn and analysed for dye concentration by UV-VIS absorbance at predetermined time intervals. The output spectra of metal halide lamp without and with UV cut-off filter (>400 nm) were presented in Fig. S3b and 3c.

2.6 Photocatalytic cyanotoxins destruction

Photocatalytic degradation of selected cyanobacterial toxins was carried out in a custom-build photo-reactor. Four non-integrated fluorescent lamps (36 W each, Philips) were used as UV light sources, as shown in Fig. S4a. 300 mg coated beads were suspended in 10 mL artificial freshwater with a toxin concentration of 10 µg·mL⁻¹. Magnetic stirring was applied to provide better diffusion. The temperature of the reactor was maintained at 25 °C by using cooling fans. Samples (200 µL) were withdrawn and analysed for remaining MC-LR by HPLC-PDA and remaining CYL by UPLC-PDA at predetermined time intervals. The output spectrum of the fluorescent lamp can be found in Fig. S4b.

2.7 HPLC analysis of MC-LR and CYL

HPLC analysis was performed on a Waters 2695 Separation Module. High-resolution photodiode array detection was performed with a Waters 2996 Photodiode Array Detector (PDA). Analysis of microcystin-LR was performed with a Symmetry C18 column 2.1 mm (inner diameter) x 150 mm with a 5 µm particle size (all Waters, UK). The mobile phases used were ultrapure water (18.2 MΩ) and acetonitrile (Fisher Scientific, UK), both containing 0.05% trifluoroacetic acid (Fisher Scientific, UK). Chromatography was achieved with a linear gradient from 15 to 75% acetonitrile over 10 min, followed by a solvent wash and equilibration. The column temperature was set to 40 °C and the flowrate applied was 0.3 mL min⁻¹. Injection volume was 25 µL. Analysis of cylindrospermopsin was performed using a reverse-phase Atlantis dC18 column 2.1 mm (inner diameter) x 150 mm with a 5 µm particle size (Waters UK). Acquity UPLC System with Xevo quadrupole time of flight (QTOF) mass spectrometry

in series (Waters, Elstree, UK) The mobile phases used were ultrapure water (18.2 M Ω) and methanol (Fisher Scientific, UK). Chromatography was achieved with a linear gradient from 2 to 10 % methanol over 10 min, followed by a solvent wash and equilibration. The column temperature was set to 40 °C and the flow rate applied was 0.3 mL min⁻¹. The resolution of the PDA was set to 1.2 nm and data was acquired over a range of 200 to 400 nm for both analytes.

3. Results and discussion

3.1 Precursors for producing *g*-C₃N₄

Three precursors thiourea (CH₄N₂S), dicyandiamide (C₂H₄N₄) and melamine (C₃H₆N₆), with increasing carbon content, were used for *g*-C₃N₄ coating. Based on previous studies on powder C₃N₄ synthesis, the formation of C₃N₄ from single carbon precursors such as urea and thiourea usually follows a continuous polymerization process with intermediate products of C₂H₄N₄ and C₃H₆N₆. The precursors sublime during the heating process and condense when forming a tri-s-triazine structure. The sublimation of the precursor or any intermediate products allows the C₃N₄ to be coated onto the glass beads substrates.

Calcination of glass beads with thiourea, dicyandiamide and melamine at 500 °C for 5 h, yielded coated C₃N₄ beads with loadings of 0.7%, 9.8% and 14.3%, respectively. Both dicyandiamide and melamine created a light-yellow coating layer upon glass beads. The glass beads calcined with thiourea showed no visible colour change. This could be expected, as thiourea, with the simplest structure, has much less chance to form polymer structure before decomposing in air. The morphologies of the coated glass beads using dicyandiamide and melamine were characterized by SEM, as shown in Fig. S5. Coating layers with rough surfaces were found on both samples. The coating layer prepared with melamine looked more porous than the one produced from dicyandiamide. Moreover, the holes on the glass beads were filled by polymer after coating indicating massive condensation during melamine sublimation.

X-ray powder diffraction was employed to check the crystal structure of the formed coating layer. The coated beads were ground into fine powder by mortar and pestle before analysis. A weak reflection peak at 27.6° was determined in *g*-C₃N₄ coated beads with both precursors (Fig. 1a). It is indexed as (002) corresponding to the aromatic stack plane.^{7, 25} The sample prepared by melamine showed a higher peak intensity. This indicated a more crystalline

structure. Moreover, the peak shifted to a higher angle, therefore, lower d spacing, which suggested tighter packing of the 2D tri-s-triazine sheets. The amorphous glass beads showed a broad bump at the low angle region. Only a small reflection peak at 26.7° was observed. More than six impurity elements in the recycled glass beads were detected. It was difficult to identify these due to the low peak intensity.

The absorbance properties of the yellow beads after coating were characterized by UV-VIS diffuse reflectance spectroscopy (Fig. 1b). Almost the same absorbance curve was found in two different precursor coated samples, with a calculated bandgap around 2.65 eV. This is close to the pure $g\text{-C}_3\text{N}_4$ reference material (2.66 eV). The same light absorption region compared to powdered $g\text{-C}_3\text{N}_4$ is expected in the photocatalysis test.

FTIR spectra revealed the chemical structure of coated $g\text{-C}_3\text{N}_4$, as shown in Fig. 1c. A small broad bump at the $3000\text{--}3500\text{ cm}^{-1}$ region was attributed to the N-H and O-H stretches from free amino groups and hydroxyl species. The strong band from 1200 to 1700 cm^{-1} resulted from stretching and vibration of C-N and C-N-C bonds.²⁶ Another sharp band observed at 806 cm^{-1} was attributed to the breathing mode of tri-s-triazine structure.²⁷

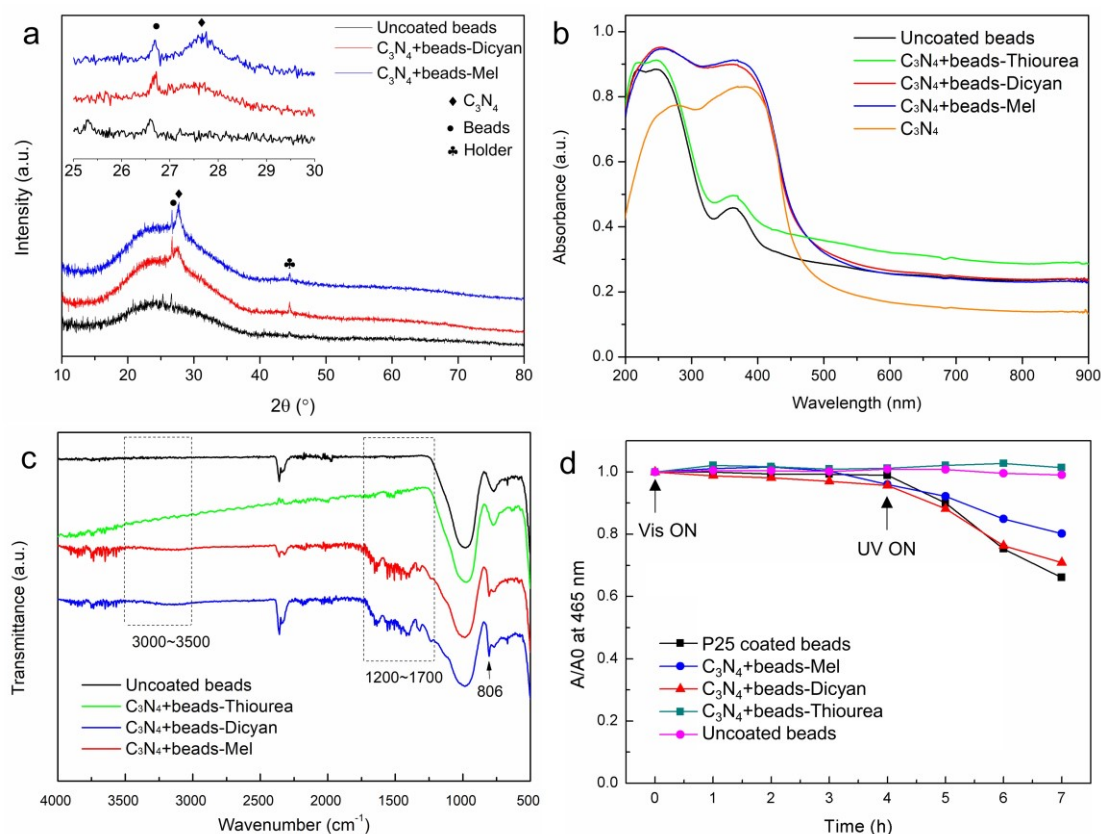


Figure 1. (a) X-ray diffraction pattern of uncoated and $g\text{-C}_3\text{N}_4$ coated beads. Insert is the detail of $g\text{-C}_3\text{N}_4(002)$ peak; (b) UV-VIS diffuse reflectance spectra of uncoated and $g\text{-C}_3\text{N}_4$ coated beads. Powder $g\text{-C}_3\text{N}_4$ was added as a reference; (c) FTIR spectra of uncoated and $g\text{-C}_3\text{N}_4$ coated beads; (d) Normalized absorption intensity at 465 nm in methyl orange degradation using different coated beads. UVCUT 400 was removed after 4 h. Samples were calcinated for 5 h at 500 °C.

All the characterizations performed confirmed the successful coating of $g\text{-C}_3\text{N}_4$ on expanded glass beads surface *via* simple calcination. The as-prepared yellow beads were used for methyl orange degradation to evaluate the photocatalytic activity. P25 coated beads were employed as a reference sample. As shown in Fig. 1d, all the samples exhibited poor photocatalytic activity under visible light ($\lambda \geq 400$ nm). Only melamine coated beads started to show dye degradation after 4 h irradiation. When switched to UV light ($\lambda \geq 250$ nm), beads coated with P25 and $g\text{-C}_3\text{N}_4$ showed activity for methyl orange removal. P25 coated beads had the best performance, followed by $g\text{-C}_3\text{N}_4$ coated beads prepared via dicyandiamide. $g\text{-C}_3\text{N}_4$ coated beads prepared with melamine showed moderate performance, while the beads prepared with thiourea showed no activity compared to uncoated beads. One possible reason for the poor activity of $g\text{-C}_3\text{N}_4$ coated beads under visible light is low light absorption. The UV-Vis absorbance curve shows coated beads have an absorption edge around 460 nm, however, the maximum absorption appears until 370 nm. This means when using a UV cut filter (≥ 400 nm), the light-harvesting on the $g\text{-C}_3\text{N}_4$ surface is much lower than when not using a filter. A 20% decrease of relative light intensity was also determined when checking the output spectrum with the spectrometer, which is another factor that causes low activity under visible light.

Although the dicyandiamide prepared $g\text{-C}_3\text{N}_4$ coating layer showed better dye degradation performance under UV light, more shedding of the photocatalyst from the glass beads into the solution was observed during the test under continuous stirring. Considering the high yield and mechanical stability, melamine seems to be a better precursor for $g\text{-C}_3\text{N}_4$ coating onto expanded glass beads.

3.2 Influence of calcination temperature

In our previous study, we found the calcination temperature in bulk $g\text{-C}_3\text{N}_4$ synthesis had a significant influence on photocatalytic performance by affecting the crystal structure and electronic structure of $g\text{-C}_3\text{N}_4$. Therefore, the calcination temperature for $g\text{-C}_3\text{N}_4$ coating was also optimized in this work.²⁵ Samples were prepared at 450 to 600 °C for 5 h with the same amount of melamine.

As shown in Fig. 2a, the peak intensity at (002) increased when the temperature rose from 450 °C to 500 °C. An obvious peak shift to a higher angle in terms of lower d spacing was observed at 500 °C. Both indicated improved crystallization with tighter packed 2D polymer sheets. When the temperature reached 550 °C, the peak intensity decreased, which may be because the polymer structure started to decompose after 500 °C. This was confirmed by thermogravimetric analysis (TGA) when heating bulk $g\text{-C}_3\text{N}_4$ in air, as shown in Fig. S6. Due to this thermal decomposition, no reflection peak of $g\text{-C}_3\text{N}_4$ was detected in samples prepared at 600 °C, which meant most of the coated $g\text{-C}_3\text{N}_4$ was burned off. The surface morphologies of these coated glass beads characterized by SEM showed this change in Fig. S7.

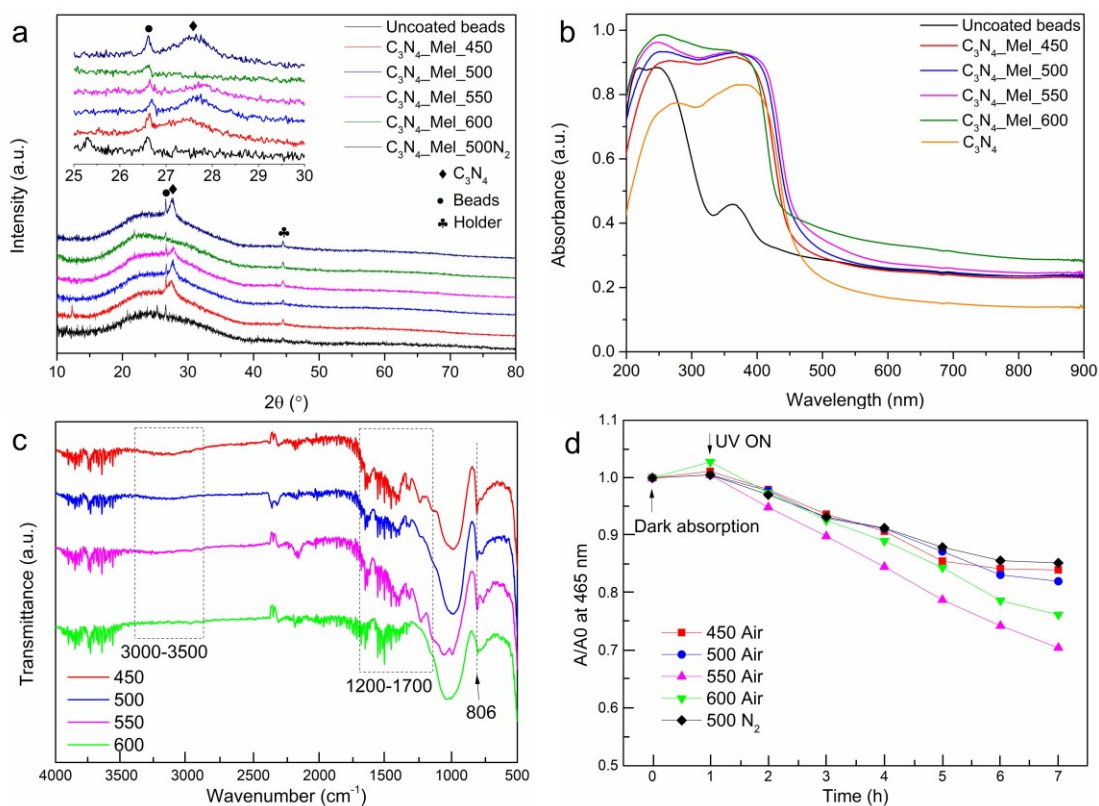


Figure 2. (a) X-ray diffraction pattern of uncoated and $g\text{-C}_3\text{N}_4$ coated beads using melamine at different temperatures. Insert is the detail of $g\text{-C}_3\text{N}_4(002)$ peak; (b) UV-VIS diffuse reflectance

spectra of uncoated and g-C₃N₄ coated beads at different temperatures. Powder g-C₃N₄ was added as a reference; (c) FTIR spectra of g-C₃N₄ coated beads at different temperatures; (d) Normalized absorption intensity at 465 nm in methyl orange degradation using coated beads prepared at different temperatures. UV light was switched on after 1 h dark absorption.

UV-Vis absorbance of coated beads presented a redshift as temperature increased from 450 °C to 550 °C (Fig. 2b). This suggested that a high annealing temperature is beneficial to form the crystalline structure of g-C₃N₄, though parts of the polymer had been decomposed at 550 °C. The sample prepared at 600 °C showed a blue shift as the decomposition domains and left little active material. Similar details were observed in the FTIR spectra in Fig. 2c. The sharp band at 806 cm⁻¹ attributed to tri-s-triazine breathing mode showed the highest intensity at 550 °C and almost disappeared at 600 °C.

Methyl orange degradation was carried out to evaluate the photocatalytic performance of coated beads. As shown in Fig. 2d, the sample prepared at 550 °C showed the highest activity under UV light. It is surprising here that the sample calcined at 600 °C showed better performance than the beads prepared at a lower temperature (450 and 500 °C) though much less of the g-C₃N₄ remained. This suggests the amount of active material may not be a key factor for photocatalytic activity because the reaction only occurs at the surface with incident light irradiation. A sample prepared in an N₂ atmosphere at 500 °C was used for comparison here to elucidate the influence of the gas atmosphere. No obvious difference from a sample prepared in the air at the same temperature was observed. Good recycling performance was found when using g-C₃N₄ coated glass beads prepared at 550 °C for methyl orange degradation, as shown in Fig. S8.

3.3 Catalysts distribution on glass beads

EDS mapping was employed to check the elemental distribution on coated glass beads. g-C₃N₄ coated beads presented uniform distribution of the N element layer on the top surface, as shown in Fig. 3c. Moreover, the N signal was detected inside the bulk of the beads. This revealed that intermediate products generated during g-C₃N₄ formation diffused through the pores and condensed. This was a major difference to P25 coated glass beads in regard to active

material distribution. Most of the coated P25 was located on the glass beads surface, as shown in Fig. S9. A thin layer containing Ti and O distributed uniformly on glass beads surface. XRD and UV-VIS absorbance confirmed the existence of the TiO_2 phase. The backbone of the porous beads mainly contained Na, Si, Ca and O, as shown in both P25 and $g\text{-C}_3\text{N}_4$ coated beads.

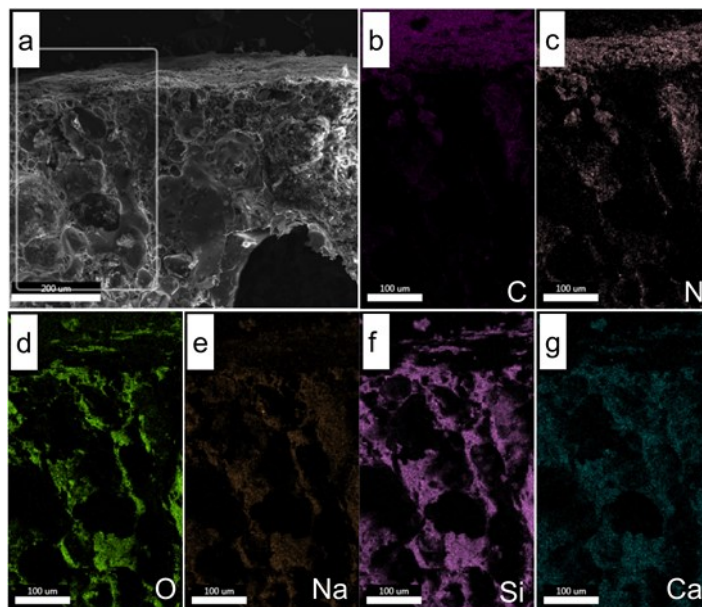


Figure 3. EDS mapping of $g\text{-C}_3\text{N}_4$ coated glass beads at a cross-section. The sample was prepared with melamine at 550 °C, 5 h. Scale bar is 200 µm in (a) and 100 µm in (b-g).

3.4 Photocatalytic removal of cyanobacterial toxins

The results obtained from both photocatalysts in the decomposition reaction of MC-LR and CYL are summarised in Fig. 4. In both cases, the coated beads were immersed in the solution containing the toxin for ten minutes in the dark for equilibration and allowing for dark absorption, before the commencement of irradiation. Controls are presented in the supplementary information. The $g\text{-C}_3\text{N}_4$ coated beads used in this experiment were prepared at 550 C, with loading content around 12% wt. This is almost the same amount of loading of the P25 coated glass beads. The BET surface area of $g\text{-C}_3\text{N}_4$ and P25 coated beads are $2.3 \text{ m}^2 \text{ g}^{-1}$ and $2.6 \text{ m}^2 \text{ g}^{-1}$, respectively. The N_2 adsorption-desorption isotherms were presented in Fig. S10.

In the MC-LR removal experiment, both coated beads showed about 5% toxin adsorption in dark. The reaction profiles after turning on UV light showed $g\text{-C}_3\text{N}_4$ coated beads resulted in the complete removal of MC-LR 15 min earlier than the case with P25 coated beads. Control experiments in Fig. S11 showed neither catalysts in dark solution nor toxin solution in light

without catalyst had any evidence of decomposition of the toxins.

In the case of CYL, a big difference in dark absorption was observed in the initial 10 min before photocatalysis. P25 coated beads absorbed 25% CYL while $g\text{-C}_3\text{N}_4$ coated beads absorbed 5% of the compound. The total time used for full removal of toxins was the same, which suggested the $g\text{-C}_3\text{N}_4$ coated beads had a better photocatalytic efficiency compared to the P25 coated materials for CYL removal. Again, light control and dark control experiments were carried out, with both showing no CYL removal in Fig. S12.

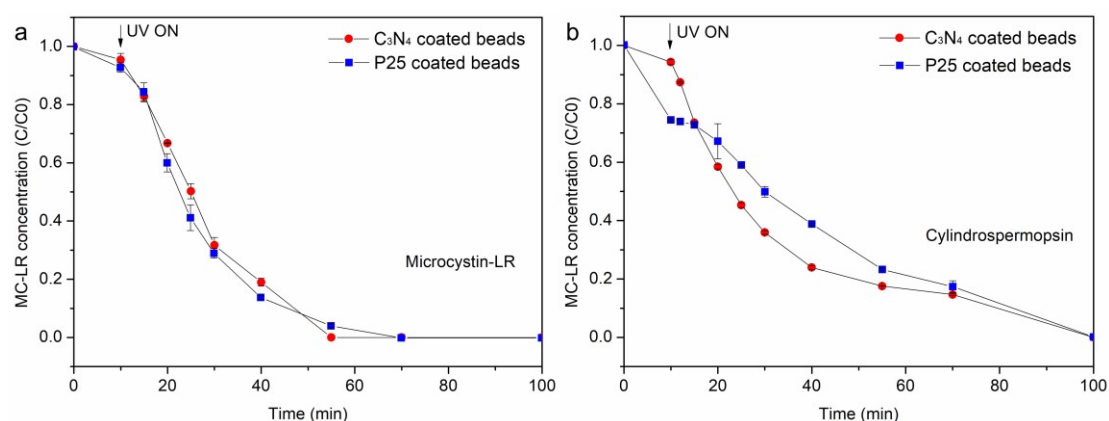


Figure 4. Graph showing the progress of photo-decomposition reactions of microcystin-LR (a) and cylindrospermopsin (b) with TiO_2 and $g\text{-C}_3\text{N}_4$ carried out at 25 °C in an open photoreactor. $g\text{-C}_3\text{N}_4$ coated glass beads in this experiment were prepared with melamine at 550 °C, 5 h.

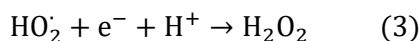
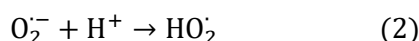
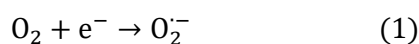
CYL is structurally very different to MC-LR lacking in any carboxylic acid groups and an oligopeptide macrocyclic structure. Due to the presence of a pendant strongly basic guanidine functionality in MC-LR, it is expected to abstract a proton from one carboxylic acid to form a zwitterion while leaving the second carboxylic acid group 'unionised'. It is well known that carboxylic acid groups have a binding affinity towards TiO_2 , thereby, making the photocatalytic process more feasible. Even without such binding functionalities CYL still underwent efficient photodecomposition with both photocatalysts. The kinetic profiles for the destruction of both toxins bore similarities despite the structural differences. It should be stressed that the absorption behaviour of CYL on the surface of $g\text{-C}_3\text{N}_4$ is less well understood than MC-LR. Nevertheless, the photocatalytic performance of $g\text{-C}_3\text{N}_4$ in the destruction process for both

toxins used in this study was comparable to TiO₂.

The weight of the catalysts was monitored before and after the test. When applying moderate stirring during the test, no obvious shedding was observed. A limited amount of g-C₃N₄ shedding was, however, still found when stirring vigorously or using an ultrasonic bath. The TEM images in Fig. S13 show different shapes of g-C₃N₄ shedding. EDS confirmed the composition are mainly C and N. Nevertheless, shedding contamination can be avoided by washing the catalysts thoroughly to remove loose-packed active materials before use.

3.5 Mechanism discussion

Although g-C₃N₄ coated glass beads have comparable performance to P25 coated ones, the mechanism for toxin removal and dye degradation are different. The photocatalytic removal of cyanobacterial toxins by TiO₂ photocatalysts has been studied previously.²⁸⁻³⁰ The photogenerated hole at the valence band reacts with water to form hydroxyl radicals (OH[•]), which have very high oxidation overpotential thus has the capacity of oxidizing a variety of organic pollutants. For g-C₃N₄, the valence band is located negative to the OH[•]/H₂O redox potential therefore unable to generate OH[•]. Only superoxide radical anions (O₂^{•-}) can be generated at the conduction band. The O₂^{•-} may subsequently react with protons (H⁺) to create H₂O₂. The generated H₂O₂ could be the source of hydroxyl radicals (OH[•]). The processes to form OH[•] have been illustrated in Fig. 5 and Eq. (1-4).



The OH[•], with a large oxidation overpotential, is believed to be the main radical that oxidizes organic pollutants during photocatalysis, though both O₂^{•-} and HO₂[•] are reactive. A comparison experiment was carried out using different quenchers in methyl orange degradation. As shown in Fig. S14, the addition of isopropanol, a OH[•] quencher resulted in a reduction of photocatalyst performance. This indicated OH[•] is essential to the degradation reaction. The addition of EDTA, a hole quencher improved the activity. This is because hole scavenger at the valence band inhibits electron-hole recombination. EDTA also introduced protons, which

promoted the reaction to create HO_2^\cdot and H_2O_2 , thus a significant performance increase was observed.

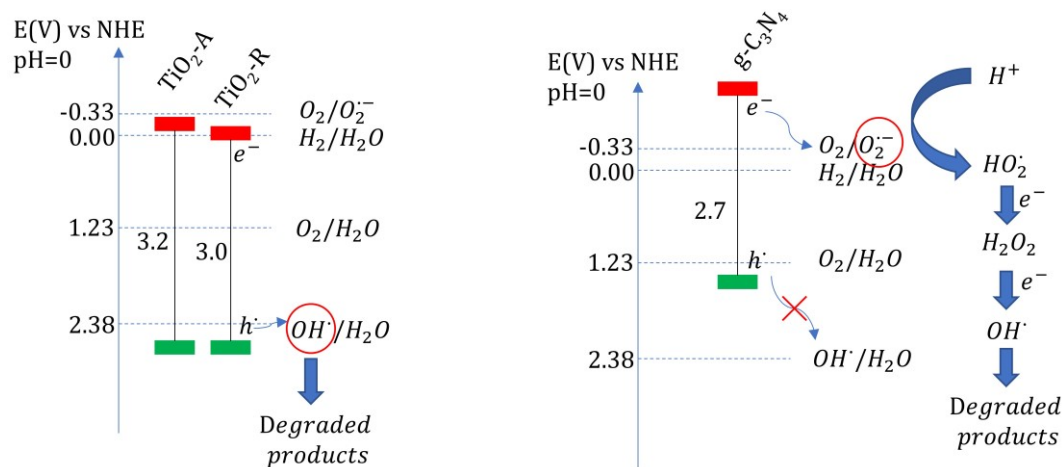


Figure 5. Proposed different mechanisms for toxin degradation in P25 and g-C₃N₄ coated glass beads.

4. Conclusions

We have demonstrated, here, the comparable performance of a simple g-C₃N₄ photocatalyst coated on floating expanded glass beads in comparison to traditional TiO₂ (P25) photocatalyst for photo-removal of MC-LR and CYL from water. It must be stressed this simple g-C₃N₄ is devoid of any detrimental metals and their insolubility in water makes it attractive materials for water purification. The floating material made recovery of the photocatalysts relatively easy which would allow for subsequent reuse. Moreover, the facile preparation process enables large batch production for full-scale application.

Acknowledgements

We acknowledge the funding provided by the Engineering and Physical Sciences Research Council, UK (Global Challenge Research Fund: EP/P029280/1) towards carrying out this research. We also thank the support on electron microscopes from EPSRC Capital for Great Technologies (Grant EP/LP017008/1 and EP/R02375/1).

References

1. K. Sivonen, in *Encyclopedia of Microbiology (Third Edition)*, ed. M. Schaechter, Academic

Press, Oxford, 2009, DOI: <https://doi.org/10.1016/B978-012373944-5.00005-5>, pp. 290-307.

2. I. Chorus and J. Bartram, *Toxic Cyanobacteria in Water: A guide to their public health consequences, monitoring and management*. 1999.
3. J. Fastner, R. Heinze, A. R. Humpage, U. Mischke, G. K. Eaglesham and I. Chorus, *Toxicon*, 2003, **42**, 313-321.
4. L. A. Lawton and P. K. J. Robertson, *Chemical Society Reviews*, 1999, **28**, 217-224.
5. M. Pirhashemi, A. Habibi-Yangjeh and S. Rahim Pouran, *J Ind Eng Chem*, 2018, **62**, 1-25.
6. M. Shekofteh-Gohari, A. Habibi-Yangjeh, M. Abitorabi and A. Rouhi, *Critical Reviews in Environmental Science and Technology*, 2018, **48**, 806-857.
7. F. Fina, S. K. Callear, G. M. Carins and J. T. S. Irvine, *Chemistry of Materials*, 2015, **27**, 2612-2618.
8. A. Akhundi, A. Badiei, G. M. Ziarani, A. Habibi-Yangjeh, M. J. Muñoz-Batista and R. Luque, *Mol Catal*, 2020, **488**.
9. X. Wang, K. Maeda, A. Thomas, K. Takanabe, G. Xin, J. M. Carlsson, K. Domen and M. Antonietti, *Nature Materials*, 2009, **8**, 76-80.
10. S. C. Yan, Z. S. Li and Z. G. Zou, *Langmuir*, 2009, **25**, 10397-10401.
11. Y. Cui, Z. Ding, P. Liu, M. Antonietti, X. Fu and X. Wang, *Physical Chemistry Chemical Physics*, 2012, **14**, 1455-1462.
12. C. Huang, W. Zhang, Z. Yan, J. Gao, W. Liu, P. Tong and L. Zhang, *RSC Advances*, 2015, **5**, 45368-45375.
13. F. Zhang, L. Wang, M. Xiao, F. Liu, X. Xu and E. Du, *Journal of Materials Research*, 2018, **33**, 201-212.
14. J. Song, X. Wang, J. Ma, X. Wang, J. Wang and J. Zhao, *Applied Catalysis B: Environmental*, 2018, **226**, 83-92.
15. J. Song, X. Wang, J. Ma, X. Wang, J. Wang, S. Xia and J. Zhao, *Chem Eng J*, 2018, **348**, 380-388.
16. Y. Xu, B. Hu, J. Liu, K. Tao, R. Wang, Y. Ren, X. Zhao, J. Xu and X. Song, *Journal of the American Ceramic Society*, 2019, **103**, 1281-1292.
17. G. E. Schaumann, A. Philippe, M. Bundschuh, G. Metreveli, S. Klitzke, D. Rakcheev, A. Grun, S. K. Kumahor, M. Kuhn, T. Baumann, F. Lang, W. Manz, R. Schulz and H. J. Vogel, *Sci Total Environ*, 2015, **535**, 3-19.
18. A. Praetorius, M. Scheringer and K. Hungerbuhler, *Environ Sci Technol*, 2012, **46**, 6705-6713.
19. Z. Xing, J. Zhang, J. Cui, J. Yin, T. Zhao, J. Kuang, Z. Xiu, N. Wan and W. Zhou, *Applied Catalysis B: Environmental*, 2018, **225**, 452-467.
20. S. Zhang, H. Li and Z. Yang, *Materials Technology*, 2017, **33**, 1-9.
21. J. Lv, T. Sheng, L. Su, G. Xu, D. Wang, Z. Zheng and Y. Wu, *Applied Surface Science*, 2013, **284**, 229-234.
22. S. Singh, H. Mahalingam and P. K. Singh, *Applied Catalysis A: General*, 2013, **462-463**, 178-195.
23. C. Edwards, L. A. Lawton, S. M. Coyle and P. Ross, *J Chromatogr A*, 1996, **734**, 163-173.
24. J. Akkanen and J. V. K. Kukkonen, *Aquat Toxicol*, 2003, **64**, 53-61.
25. M. Caux, F. Fina, J. T. S. Irvine, H. Idriss and R. Howe, *Catalysis Today*, 2017, **287**, 182-188.
26. X. Yang, F. Qian, G. Zou, M. Li, J. Lu, Y. Li and M. Bao, *Applied Catalysis B: Environmental*, 2016, **193**, 22-35.

- 446 27. X. Bai, L. Wang, Y. Wang, W. Yao and Y. Zhu, *Applied Catalysis B: Environmental*, 2014, **152-**
447 **153**, 262-270.
- 448 28. L. A. Lawton, P. K. J. Robertson, B. J. P. A. Cornish, I. L. Marr and M. Jaspars, *Journal of*
449 *Catalysis*, 2003, **213**, 109-113.
- 450 29. C. J. Pestana, C. Edwards, R. Prabhu, P. K. J. Robertson and L. A. Lawton, *J Hazard Mater*,
451 2015, **300**, 347-353.
- 452 30. L. X. Pinho, J. Azevedo, Â. Brito, A. Santos, P. Tamagnini, V. J. P. Vilar, V. M. Vasconcelos and
453 R. A. R. Boaventura, *Chem Eng J*, 2015, **268**, 144-152.
- 454